

A Comparative Analysis of Photospheric Bright Points in an Active Region and in the Quiet Sun

P. Romano · F. Berrilli · S. Criscuoli · D. Del Moro ·
I. Ermolli · F. Giorgi · B. Viticchié · F. Zuccarello

Received: 15 November 2011 / Accepted: 20 January 2012
© Springer Science+Business Media B.V. 2012

Abstract We present a comparative study of photometric and dynamic properties of photospheric bright points (BPs) observed at the disk centre in the active region (AR) NOAA

Advances in European Solar Physics

Guest Editors: Valery M. Nakariakov, Manolis K. Georgoulis, and Stefaan Poedts

P. Romano (✉)

INAF – Catania Astrophysical Observatory, Via S. Sofia 78, 95123 Catania, Italy
e-mail: prom@oact.inaf.it

F. Berrilli · D. Del Moro

Dipartimento di Fisica, Università degli Studi di Roma Tor Vergata, via della Ricerca Scientifica 1,
00133 Roma, Italy

F. Berrilli

e-mail: berrilli@roma2.infn.it

D. Del Moro

e-mail: delmoro@roma2.infn.it

S. Criscuoli · I. Ermolli · F. Giorgi

INAF – Osservatorio Astronomico di Roma, via Frascati 33, 00040 Monte Porzio Catone, Italy

S. Criscuoli

e-mail: criscuoli@oaroma.inaf.it

I. Ermolli

e-mail: ermolli@oaroma.inaf.it

F. Giorgi

e-mail: giorgi@oaroma.inaf.it

B. Viticchié

ESA/ESTEC RSSD, Keplerlaan 1, 2200 AG Noordwijk, The Netherlands

e-mail: bartolomeo.viticchie@esa.int

F. Zuccarello

Dipartimento di Fisica e Astronomia, Sezione Astrofisica, Università di Catania, via S. Sofia 78, 95123
Catania, Italy

e-mail: fzu@oact.inaf.it

10912 and in the quiet Sun. We found that the average concentration of BPs is 54% larger in the AR than in the quiet Sun. We also measure a decrease of the BP concentration and an increase of their size moving away from the AR centre. However, these variations can be ascribed to the variation of the spatial resolution and image quality in the field of view of the AR dataset. We also found that BPs in the quiet Sun are associated with larger downflow motions than those measured within the AR. Finally, from our measurements of contrast and velocity along the line of sight, we deduced that BPs are less bright in high magnetic flux density regions than in quiet regions, due to a lower efficiency of convection in the former regions.

Keywords Magnetic fields, photosphere · Velocity fields, photosphere

1. Introduction

High resolution G-band images of the photosphere show tiny bright features with a diameter less than 300 km, called bright points (BPs). They are usually located in the intergranular dark lanes (Title, Tarbell, and Topka, 1987) and are concentrated in active regions (ARs) or at the border of the supergranules in the quiet Sun (QS) (Sánchez Almeida *et al.*, 2004). BPs are associated with strong magnetic field concentrations of about 1.5×10^3 G (Beck *et al.*, 2007; Viticchié *et al.*, 2010). Numerical simulations (Carlsson *et al.*, 2004; Steiner, 2005; Shelyag *et al.*, 2007; Danilovic, Schüssler, and Solanki, 2010) show that these small-scale concentrations of magnetic flux derive from the interaction between magnetic fields and convective motions. It is also known that magnetic flux concentrations may suppress convection in ARs. In this regard, Morinaga *et al.* (2008) found that the concentration of magnetic flux tubes is more relevant than the flux strength to the suppression of convection. Ishikawa *et al.* (2007) proposed variations of convective efficiency to be the cause of the different photometric properties measured on BPs observed in ARs and in QS regions. Both phenomena are of great relevance for solar irradiance studies. In fact, convection is a mechanism by which energy is transported to the solar surface, and a variation of its efficiency, induced for instance by the temporal variation of the global properties of the solar magnetic field, might contribute to solar irradiance variations, especially at long-term time scales. On the other hand, if the variation of the efficiency of convection determines the radiative energy outputs of magnetic elements (see also Kobel, Solanki, and Borrero, 2011), the contribution of these to irradiance variations might not be constant with time. This mechanism has been recently proposed by Harder *et al.* (2009) to explain results of spectral irradiance variations measured in the visible and infrared spectral ranges.

As the suppression of convective motions occurs at small spatial scales, at least comparable with the best spatial resolution that can be achieved by modern instrumentation, these phenomena have been poorly investigated.

The aim of this study is to investigate the variation of photometric and dynamic properties of photospheric BPs with the variation of the magnetic flux density in regions of the centre of the solar disk characterized by different degrees of magnetic flux densities. To this aim, we analysed two high spectral, spatial, and temporal resolution datasets imaging AR NOAA 10912 and a QS region. The datasets and analysis methods are described in Sections 2 and 3. Our main findings are presented in Section 4, with concluding remarks in Section 5.

2. Data

In this study we analysed two datasets acquired with the *Interferometric Bidimensional Spectrometer* (IBIS) instrument (Cavallini, 2006) at the National Solar Observatory (NSO) *Dunn Solar Telescope* (DST) on 2 October and 21 November 2006. The first set consists of 120 spectral scans of the Fe I 709.0 nm line of AR NOAA 10912 (AR dataset, hereinafter). This AR is a small magnetic bipolar region observed at the centre of the solar disk (N7.2W3.1), which was also studied by Contarino *et al.* (2009). In this set each scan contains 1024×1024 pixel images obtained at 29 spectral points in the line, with a pixel scale of $0.085 \text{ arcsec pixel}^{-1}$, a field of view (FOV) of about $57 \times 61 \text{ arcsec}^2$, an exposure time of 80 ms, and 20 s cadence. The second dataset, also described in Viticchié *et al.* (2010), consists of 50 spectro-polarimetric scans of the Fe I 630.25 nm line of a QS region at the disk centre (QS dataset, hereinafter). In this set each scan contains 256×256 pixel images obtained at 45 spectral points in the line, a pixel scale of $0.17 \text{ arcsec pixel}^{-1}$, an FOV of about $43 \times 43 \text{ arcsec}^2$, an exposure time of 80 ms, and 89 s cadence. The two datasets span about 70 min and 41 min, respectively. Both datasets are complemented by white light (WL) and G-band images that were taken simultaneously to the spectral data by approximately imaging their FOV. The WL images have the same spatial resolution of the corresponding spectral data, while the G-band images have the same pixel scale of the spectral images for the first dataset and a pixel scale four times smaller than that of the spectral images for the second dataset.

During the acquisition of both datasets the image quality was stabilized by the adaptive optics (AO) system of the telescope (Rimmele, 2004), tracking in both cases the centre of the FOV. In particular, the seeing conditions during the acquisition of the QS dataset allowed us to achieve the diffraction limit for the first 34 scans and very good quality for the first eight scans of the AR dataset.

3. Analysis

The calibration of IBIS spectral data included dark- and flat-field correction, multi-frame blind deconvolution (MFBD) restoring (Van Noort, Rouppe van der Voort, and Löfdahl, 2006) of WL images, and reconstruction of spectral images by re-scaling, rotating, shifting, and de-stretching them to their restored WL counterparts. G-band images were independently corrected for dark and flat field, and restored by MFBD. In particular, the restoration was performed so that approximately eight and ten G-band frames were available for each spectral scan of the AR and QS datasets, respectively. Figures 1(a) and (c) show examples of G-band restored frames from the two datasets.

After analysing the rms contrast and spatial resolution, we selected one of the best quality scans for each dataset (*i.e.* the one acquired during the best seeing conditions). The BPs were identified in the G-band images corresponding to the best quality scans by applying the Multi Level Thresholding 4 (MLT4) algorithm (Bovelet and Wiehr, 2007), with the *unitary cut level* set to 0.63 and 0.40 for the first and the second dataset, respectively. These values allowed us to derive segmented images with realistic patterns of solar features and slightly broadened intergranular lanes for each dataset. Then, according to the method used by Bovelet and Wiehr (2008), we removed from further analysis all larger size features with local G-band enhancements occasionally embedded, which are known to be non-magnetic (Langhans, Schmidt, and Tritschler, 2002). This selection is performed by taking into account only intergranular features with an area $\leq 0.1 \text{ Mm}^2$ (30 pixels) and $\leq 0.06 \text{ Mm}^2$

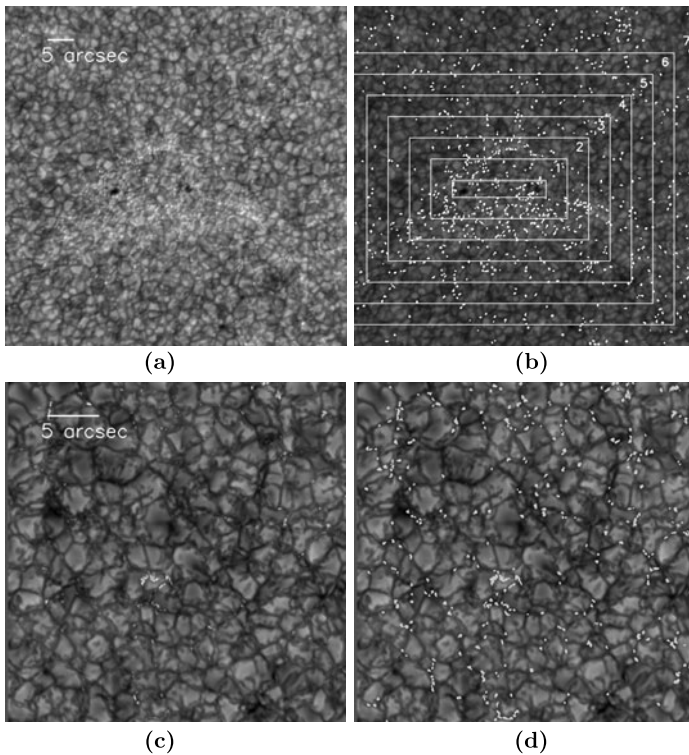


Figure 1 (a) G-band image of the AR NOAA 10912; the FOV is $68 \times 68 \text{ arcsec}^2$. (b) G-band image of the AR with the BPs identified by the MLT4 overlaid in white. The boxes indicate the subfields considered in the analysis of the BP properties as functions of the BP distance from the centre of the bipole of the AR. (c) G-band image of the QS area at the centre of the solar disk; the FOV is $34 \times 34 \text{ arcsec}^2$. (d) G-band image of the QS area with the BPs identified by the MLT4 overlaid in white.

(75 pixels) for the AR and QS datasets, respectively. Figures 1(b) and (d) show an example of the G-band images of the two datasets with the BPs identified by the MLT4 overlaid in white. To study the variation of the BP properties as a function of the distances of the BPs from the magnetic bipole of the AR and to compare the properties derived from the two datasets, we divided the FOV of the AR dataset into seven different shells, as shown in Figure 1(b). We considered the bipole centred into a box of 200×40 pixels ($\sim 12.3 \times 2.5 \text{ Mm}^2$) with a 50 pixel ($\sim 3.1 \text{ Mm}$) width for each shell.

The line-of-sight (LOS) velocity fields were estimated using Doppler shifts of the cores of the 709.0 nm and 630.2 nm spectral lines for the AR and QS datasets, respectively. In order to discuss the obtained results, we computed the velocity response functions of the cores of both lines by means of the RH synthesis code (Uitenbroek, 2002), through the facular Model P of Fontenla *et al.* (2009). We found that both response functions sample quite wide ranges of the lower photosphere and mostly overlap (see also Khomenko and Collados, 2007 and Watanabe *et al.*, 2010 for a further discussion of the formation heights of 630.2 nm and 709.0 nm lines in magnetic features), thus suggesting that differences obtained between the two datasets are probably not ascribed to the different formation heights of the two lines.

Note that the two datasets are characterized by different spatial sampling, spatial resolution, and scattered light level. As these differences affect the measured properties of BPs (see *e.g.* Utz *et al.*, 2009; Viticchié *et al.*, 2010; and Crisculi and Rast, 2009), we also compared the results derived from the two datasets with those obtained in a G-band frame of the QS dataset that was degraded (QS-degraded, hereafter) to match the image quality of the AR frame. In particular, the QS frame was convolved with a point spread function (PSF) described by the sum of a Gaussian and a Lorentzian function and re-sampled to the same pixel scale of the AR frame. The free parameters of the PSF were chosen so that the rms contrast of the solar granulation in the QS-degraded frame matched that measured in a quiet region in the AR frame. Note that the quiet region in the AR frame considered for this purpose was selected far from the bipolar region and included the three outermost shells indicated in Figure 1. Therefore, due to the worsening efficiency of the AO in compensating for atmospheric seeing with increasing distance from the lock point, the QS-degraded frame represents better the quality of the outer regions, rather than that of the innermost parts, of the AR frame. Finally, we applied the MLT4 algorithm in the QS-degraded frame by using the same parameters considered for the AR G-band image and analysed the obtained results.

4. Results

4.1. Density

The MLT4 method singled out about 820 and 381 BPs in the G-band images of the AR and QS frames, respectively. Taking into account the different FOVs and spatial resolutions of the two datasets, we obtained mean BP concentrations of about 0.34 and 0.43 BPs Mm^{-2} in the AR and QS frames, respectively. In the QS-degraded frame we measured a concentration of about 0.22 BPs Mm^{-2} , thus indicating that the average concentration of BPs in the AR is about 54% larger with respect to that measured in the QS region.

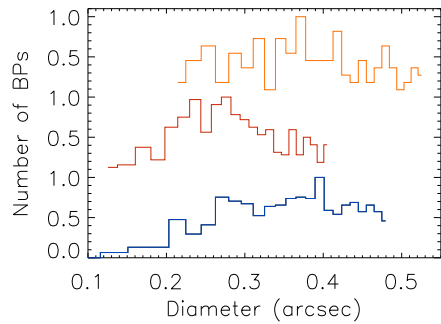
We then analysed the BP concentration in the seven shells reported in Figure 1(b). The results are summarized in Table 1. We found that the BP concentration decreases from the region near the bipole to the boundary of the FOV. In particular, we found a BP concentration comparable with that measured in the QS region starting from the fifth shell, *i.e.* for distances larger than 0.76 Mm from the bipole centre. The concentration of BPs in the innermost shell is approximately 4.5 times larger than that found in the outermost shells, and is

Table 1 BP properties in the shells of the AR G-band image of Figure 1(a).

Subfield	Number of BPs	Area FOV (Mm^2)	Concentration (BP Mm^{-2})	$\langle D \rangle^a$ (arcsec)	Peak of D (arcsec)	(Contrast)
1	138	136.715	1.00	0.34	0.29	1.0827
2	133	212.668	0.62	0.39	0.32	1.0856
3	108	288.621	0.37	0.35	0.38	1.0365
4	109	364.574	0.30	0.37	0.35	1.0254
5	79	399.512	0.20	0.37	0.37	1.0193
6	88	387.359	0.23	0.36	0.42	1.0217
7	136	607.623	0.22	0.38	0.38	1.0329

^aAverage BP diameter.

Figure 2 Size distribution of the analysed BPs in the AR (blue), in the QS (red), and in the QS-degraded (orange) G-band frames. The number of BPs is normalized to the maximum of each distribution.



approximately 2.3 times larger than that found in the QS frame. Due to the different image quality over the FOV of the AR frame, these values most likely bracket the real one.

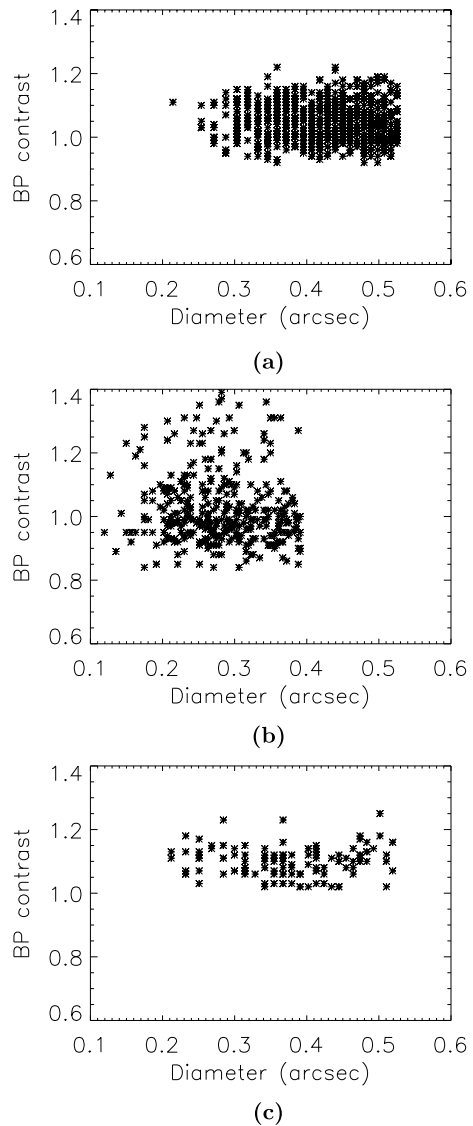
4.2. Size

We analysed the size of the BPs identified in the three frames and in each subarea of the AR image. The distributions of the diameters, D , of the BPs (estimated from the area by assuming BPs to be circularly symmetric features) are shown in Figure 2. We found that the distribution of BP sizes for the AR frame is broader than that derived from the QS frame; in particular, the distribution of the former is also populated at sizes larger than 0.4 arcsec. The peaks of the distributions calculated in the AR and QS datasets are at 0.45 and 0.25 arcsec, respectively. The peak of the distribution obtained in the QS-degraded frame is 0.37 arcsec, and its shape more closely resembles that derived from the analyses of the AR frame. These results suggest that the different values measured in the AR and QS regions must be primarily ascribed to the different image quality of the two datasets. This is also confirmed by the fact that, as reported in Table 1, the peak positions of the distributions of the BP diameters increase with the distance from the bipole. Therefore, larger BP dimensions are measured in regions characterized by worse image quality. Indeed, the peak of the distribution of diameters in the innermost shell is comparable with the one measured in the QS dataset. However, the average of the BP diameters does not appreciably vary with the distance from the bipole. The average of the BP diameters in the whole FOV of the AR is 0.37 arcsec, corresponding to an area of about 0.057 Mm^2 , whereas the average BP diameter for the QS G-band images is 0.30 arcsec, corresponding to an area of about 0.036 Mm^2 .

4.3. Photometric Properties

The photometric properties of the BPs are reported in Figure 3, showing the variation of the average G-band contrast with respect to the size of BPs measured in the three frames. The contrast here is defined as the ratio between the average intensity of each identified BP and the average intensity in a subregion devoid of BPs and selected from the corresponding frame. The plots show that the G-band contrast of BPs is independent of the size. Nevertheless, the average BP contrast and the dispersion of the measurements obtained from the QS region are higher than those derived from the AR frame. These differences are reduced when comparing results obtained in the QS-degraded and AR frames, *i.e.* when taking into account the different spatial resolution and scattered light level in the two datasets. (See for instance Criscuoli and Ermolli, 2008; and Wedemeyer-Böhm and Rouppe van der Voort, 2010 for further discussions on the effects of stray light on the measurement of the contrast

Figure 3 BP contrast vs. diameter in the selected G-band images of the AR (a) and QS (b) and in the degraded G-band image of the QS (c). The BP contrast is defined as the ratio between the average intensity of each identified BP and the average intensity in a subregion devoid of BPs and selected from the corresponding frame.



of the features.) In particular, we measured average contrasts of 1.05 and 1.09, and standard deviations of 0.06 and 0.05, for the BPs singled out in the AR and QS frames, respectively. Although these differences are small, they confirm the findings of Ishikawa *et al.* (2007), according to which higher BP contrast is expected in regions characterized by lower magnetic flux. The decrease of the average contrast with the increase of the distance from the AR bipole reported in Table 1 is most likely ascribed to the decrease of the spatial resolution toward the edges of the frame. Nevertheless, we notice that, in spite of the decrease in the image quality, the contrast of BPs slightly increases in the two outermost shells.

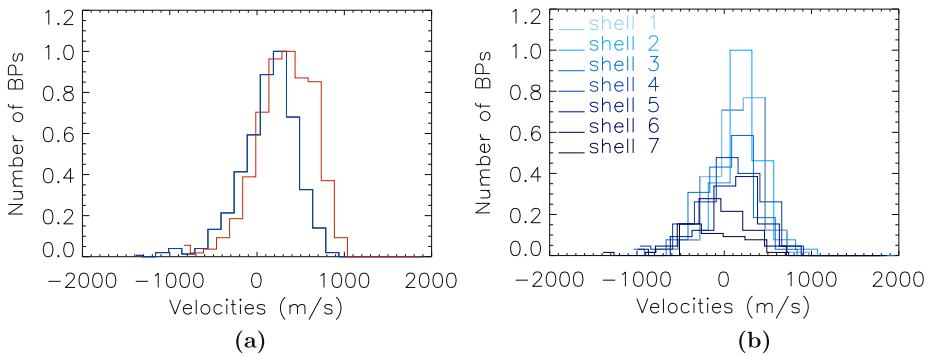


Figure 4 (a) Histogram of the BP LOS velocities derived from the Doppler shift of line cores for the AR (blue line) and QS (red line) datasets, respectively. (b) Histogram of the BP LOS velocities derived from the Doppler shift of the Fe I line at 709.0 nm in the seven shells of Figure 1(b). Positive velocities indicate redshifts (downflow motions).

4.4. Line-of-Sight Velocity

Results obtained from the analysis of the LOS velocities are displayed in Figure 4. Figure 4(a) shows the v_{LOS} histograms for the BPs observed in the AR and QS datasets. By convention, positive velocities indicate redshifts (downflow motions). The most evident difference between the two distributions is the larger population of downflow velocities found for the QS dataset. Moreover, the velocity distribution for the AR is narrower than the distribution for the QS, probably due to the better pixel sampling of the spectral scan of the first dataset. The peaks of the velocity distribution for the BPs of the AR and the QS are at about 250 m s^{-1} and 350 m s^{-1} , respectively. The two distributions are associated with average downflow motions of 210 and 395 m s^{-1} for the AR and QS datasets, respectively. Note that 23% and 9% of the analysed BPs in the QS and in the AR have upflows. In order to verify that the differences between the two distributions were not due to the different pixel sampling of the two datasets, we re-sampled the AR spectral data to the pixel scale of the QS spectral data and found that the velocity distribution (not shown) in the re-sampled dataset is broader and peaks toward smaller velocities than the original distribution. This result suggests that the contribution at negative velocity populations of both distributions in Figure 4(a) might come from not fully resolved features. This is also confirmed by the results displayed in Figure 4(b), which shows the variation of the BP v_{LOS} distributions in the seven shells of the AR images. We note that with the increase of the distance from the bipole, *i.e.* with the decrease of the spatial resolution, the positions of the peaks of the distributions gradually decrease, while the widths of the distributions increase. In particular, in the sixth and seventh shells the peaks of the distributions are located at negative velocities (*i.e.* upflow motions).

5. Discussion

The results presented in this work provide further information on the concentration, size, contrast, and LOS velocity of the BPs in regions of the photosphere characterized by different magnetic flux densities. In particular, we compared the properties of BPs singled out in

G-band frames, imaging an active region (AR NOAA 10912) and a quiet Sun region (QS), both located close to disk centre.

The first result we found is the different BP concentration in the two FOVs. In fact, by setting the two analysed G-band frames to the same spatial sampling and image quality, we found that in the AR the average concentration of BPs is 54% larger than in the QS. Moreover, the distribution of BPs is not uniform over the AR. Analysing of the spatial distribution of BPs within the FOV of the AR, we estimated the concentration of BPs at the core of the AR to be between 4.5 and 2.3 times larger than at its periphery. We also note that the concentration value of 0.43 BPs Mm^{-2} found for the QS data is higher than the majority of values reported in previous studies (e.g. Sánchez Almeida *et al.*, 2004; de Wijn *et al.*, 2005; and Bovelet and Wiehr, 2008), but is quite low with respect to the recent estimates of Sánchez Almeida *et al.* (2010) and Andić *et al.* (2011), who found concentrations of 0.98 BPs Mm^{-2} and 2.8 BPs Mm^{-2} , respectively. The differences between the results of the various authors must be partly ascribed to the different spatial resolutions of the data analysed, but also to the different techniques employed to single out the features in the images, as also discussed in Sánchez Almeida *et al.* (2010).

We also investigated the distributions of sizes of BPs singled out in the two datasets. We found that the observed differences, as well as the variations of BP sizes with the increase of the distance from the core of the AR reported in Table 1, must be ascribed to spatial resolution and image quality effects (see also Utz *et al.*, 2009). From the QS dataset, which is characterized by better spatial resolution, we found a typical size of 0.25 arcsec, *i.e.* approximately 175 km. This value is in agreement with values reported by authors who observed BPs in quiet regions (as for instance Sánchez Almeida *et al.*, 2004; Utz *et al.*, 2009; or Crockett *et al.*, 2010) or active regions (as for instance Beck *et al.*, 2007; Berger, Rouppe van der Voort, and Löfdhal, 2007; Wiehr, Bovelet, and Hirzberger, 2004), thus corroborating our conclusions. The same independence from the average magnetic flux of the region where BPs are located was found by Crockett *et al.* (2010) using magnetohydrodynamic simulations.

The analyses of photometric properties of BPs derived from the two datasets showed that the features identified in the QS frame are characterized by an average contrast value higher than that measured for the features identified in the AR image, even when taking into account the different spatial resolutions and scattered light level of the two datasets. This result confirms what was already found by Ishikawa *et al.* (2007) through the analysis of high spatial resolution G-band data: BPs in high magnetic flux density regions are less bright, probably due to the reduction of lateral heatflow from the surrounding plasma, which results from the decreasing efficiency of convection in the region.

Our results indicate that convection is more suppressed in BPs observed in the AR than in the QS. In particular, we found that the most likely downflow speed of BPs in the AR is 180 m s^{-1} lower than that measured in the QS. Moreover, the velocity distribution of BPs in the QS is asymmetric, with a larger population at stronger downflows and a little tail toward upflows. The distribution of velocities for BPs observed in the AR is instead more symmetric. This result is in agreement with a recent study by Narayan and Scharmer (2010) who showed that 'isolated bright points' usually have associated larger downflow motions compared with those measured within 'strings'. We also note that in both datasets the measured downflow velocities never exceeded 1.1 km s^{-1} , whereas upflow velocities were always smaller than 1.3 km s^{-1} , although larger values have recently been reported, e.g. by Berger, Rouppe van der Voort, and Löfdhal (2007) for BPs observed in an AR, or by Riethmüller *et al.* (2010) for features singled out in a QS. Ishikawa *et al.* (2007) found instead a distribution even narrower than ours. These differences are probably ascribed

not only to the different spatial resolutions, but also to the spectral lines employed for the analysis.

Finally, by studying the variation of velocity distributions within the FOV of the AR frame and the AR frame re-sampled to a worse pixel scale, we found that the reduction of spatial resolution of images generally broadens the distributions of the velocities of BPs and shifts the peak toward lower values, leading in some cases to upflow motions within the features.

Acknowledgements This work was supported by the Istituto Nazionale di Astrofisica (PRIN INAF 2010), by the Agenzia Spaziale Italiana (contract I/015/07/0), and by the Università degli Studi di Catania.

The authors wish to thank the DST staff for its support during the observing campaigns.

The authors wish to thank the referee for her/his comments and suggestions, which led to a sounder version of the manuscript.

References

- Andić, A., Chae, J., Goode, P.R., Cao, W., Ahn, K., Yurchyshyn, V., Abramenko, V.: 2011, *Astrophys. J.* **731**, 29.
- Beck, C., Bellot Rubio, L.R., Schlichenmaier, R., Sütterlin, P.: 2007, *Astron. Astrophys.* **472**, 607.
- Berger, T.E., Rouppe van der Voort, L., Löfdahl, M.: 2007, *Astrophys. J.* **661**, 1272.
- Bovelet, B., Wiehr, E.: 2007, *Solar Phys.* **243**, 121.
- Bovelet, B., Wiehr, E.: 2008, *Astron. Astrophys.* **488**, 1101.
- Carlsson, M., Stein, R.F., Nordlund, Å., Scharmer, G.: 2004, *Astrophys. J.* **610**, L137.
- Cavallini, F.: 2006, *Solar Phys.* **236**, 415.
- Contarino, L., Zuccarello, F., Romano, P., Spadaro, D., Ermolli, I.: 2009, *Astron. Astrophys.* **507**, 1625.
- Criscuoli, S., Ermolli, I.: 2008, *Astron. Astrophys.* **484**, 591.
- Criscuoli, S., Rast, M.P.: 2009, *Astron. Astrophys.* **495**, 621.
- Crockett, P.J., Mathioudakis, M., Jess, D.B., Shelyag, S., Keenan, F.P., Christian, D.J.: 2010, *Astrophys. J.* **722**, 188.
- Danilovic, S., Schüssler, M., Solanki, S.K.: 2010, *Astron. Astrophys.* **509**, 76.
- de Wijn, A.G., Rutten, R.J., Haverkamp, E.M.W.P., Sütterlin, P.: 2005, *Astron. Astrophys.* **441**, 1183.
- Fontenla, J.M., Curdt, W., Haberleiter, M., Harder, J., Tian, H.: 2009, *Astrophys. J.* **707**, 482.
- Harder, J.W., Fontenla, J.M., Pilewskie, P., Richard, E.C., Woods, T.N.: 2009, *Geophys. Res. Lett.* **36**, 911.
- Ishikawa, R., Tsuneta, S., Kitakoshi, Y., Katsukawa, Y., Bonet, J.A., Vargas Dominguez, S., Rouppe van der Voort, L.H.M., Sakamoto, Y., Ebisuzaki, T.: 2007, *Astron. Astrophys.* **472**, 911.
- Kobel, P., Solanki, S.K., Borrero, J.M.: 2011, *Astron. Astrophys.* **531**, 112.
- Khomenko, E., Collados, M.: 2007, *Astrophys. J.* **659**, 1726.
- Langhans, K., Schmidt, W., Tritschler, A.: 2002, *Astron. Astrophys.* **394**, 1069.
- Morinaga, S., Sakurai, T., Ichimoto, K., Yokoyama, T., Shimojo, M., Katsukawa, Y.: 2008, *Astron. Astrophys.* **481**, L29.
- Narayan, G., Scharmer, G.B.: 2010, *Astron. Astrophys.* **524**, 3.
- Riethmüller, T.L., Solanki, S.K., Martínez Pillet, V., Hinzberger, J., Feller, A., Bonet, J.A., Bello González, N., Franz, M., Schüssler, M., Barthol, P., *et al.*: 2010, *Astron. Astrophys.* **723**, 169.
- Rimmele, T.R.: 2004, *Proc. SPIE* **5490**, 34.
- Sánchez Almeida, J., Márquez, I., Bonet, J.A., Domingues Cardena, I.F., Muller, R.: 2004, *Astrophys. J.* **609**, 91.
- Sánchez Almeida, J., Bonet, J.A., Viticchié, B., Del Moro, D.: 2010, *Astrophys. J.* **715**, 26.
- Shelyag, S., Schüssler, M., Solanki, S.K., Vögler, A.: 2007, *Astron. Astrophys.* **469**, 731.
- Steiner, O.: 2005, *Astron. Astrophys.* **430**, 691.
- Title, A.M., Tarbell, T.D., Topka, K.P.: 1987, *Astrophys. J.* **317**, 892.
- Uitenbroek, H.: 2002, *Astrophys. J.* **565**, 1312.
- Utz, D., Hanslmeier, A., Möstl, C., Muller, R., Veronig, A., Muthsam, H.: 2009, *Astron. Astrophys.* **498**, 289.
- Van Noort, M., Rouppe van der Voort, L., Löfdahl, M.: 2006, *Astron. Soc. Pac. Conf. Ser.* **354**, 55V.
- Viticchié, B., Del Moro, D., Criscuoli, S., Berrilli, F.: 2010, *Astrophys. J.* **723**, 787.
- Watanabe, H., Tritschler, A., Kitai, R., Ichimoto, K.: 2010, *Solar Phys.* **266**, 5.
- Wedemeyer-Böhm, S., Rouppe van der Voort, L.: 2010, *Astron. Astrophys.* **503**, 225.
- Wiehr, E., Bovelet, B., Hinzberger, J.: 2004, *Astron. Astrophys.* **422**, 63.